A highorder shell finite element for the large deformation analysis of soft material structures

(Article begins on next page)

RESEARCH ARTICLE

WILEY

A high-order shell finite element for the large deformation analysis of soft material structures

A. Pagani[1] | R. Augello[1] | E. Carrera[1,2]

[1]*Mul*[2] Group, Department of Mechanical and Aerospace Engineering, Politecnico di Torino, Torino, Italy

[2]Department of Mechanical Engineering, College of Engineering, Prince Mohammad Bin Fahd University, Al Khobar, Kingdom of Saudi Arabia

Correspondence
A. Pagani, Mul2 Group, Department of Mechanical and Aerospace Engineering, Politecnico di Torino, Corso Duca degli Abruzzi 24, 10129, Torino, Italy.
Email: alfonso.pagani@polito.it

Summary

This work proposes a higher-order unified shell finite element for the analysis of cylinders made of compressible and nearly incompressible hyperelastic materials. The nonlinear governing equations are derived employing the Carrera unified formulation (CUF), thanks to which it is possible to build shell elements with the capability to capture three-dimensional (3D) transverse and out-of-plane effects. The material and geometric nonlinearities are expressed in an orthogonal curvilinear reference system and the coupled formulation of hyperelastic constitutive law is considered. The principle of virtual work and a total Lagrangian approach is used to derive the nonlinear governing equations, which are solved by a Newton–Raphson scheme. The numerical investigations deal with a curved arch and both thick and thin cylinders subjected to line and point loadings. The obtained results are validated by comparing them with those from the literature. They demonstrate the reliability of the proposed method to analyze compressible and incompressible hyperelastic shell structures.

KEYWORDS

Carrera unified formulation, finite elements, geometrical nonlinearity, higher-order shell model, hyperelastic material

1 | INTRODUCTION

Hyperelastic soft materials are widely adopted in different applications ranging in various engineering fields, from biomedical to aerospace. In general, they are used when, under the presence of high loads, a high flexibility needs to be guaranteed. Elastomeric pads in bridges, car door seals, rail pads, fluid seals and car tyres are some typical examples. For instance, in the aerospace fields, hyperelastic materials are employed to build devices with unique elastic properties, such as pressure flexible sensors.[1] In the biomedical field, soft materials are used for the simulation of natural tissues, such as sino-nasal tissue for neurosurgery simulation[2] or for the description of the behavior of the arteries.[3] The most commonly adopted constitutive models are represented by the Mooney–Rivlin and neo-Hookean strain energy functions.[4,5] They are employed for the analysis of compressible and incompressible materials, which are the two main types into which the nonlinear hyperelastic materials are classified. The static analysis of hyperelastic structures was the subject of extensive research by a number of researchers, such as Basar and Ding,[6] Tamadapu and DasGupta,[7] and Kiendl et al.[8]

Shell formulations are typically used to model specific phenomena such as the deformation of biological tissues[9,10] and wrinkling membranes.[11–13] Since the first derivation of the theory by Love,[14] the governing equations and the

related numerical implementation of shells was a challenging task for scientists. Large deformations most likely appear in thin shells, and a geometrical linear approach is not able to describe such phenomena. Therefore, thin shells are often described using a geometrical nonlinear approach. Many studies have applied the St. Venant-Kirchhoff constitutive model, which leads to reliable results when shells are subjected to large displacements, but not in the case of large strains. Thus, for thin shells that undergo both large displacements and strains, the hyperelastic constitutive model must be included to capture their static response.

In recent decades, a remarkable effort on soft and hyperelastic shell structures was dedicated by scientists and engineers, due to their potential application to biomaterials. A few works are mentioned hereafter. Basar and Ding,[6] starting from a quadratic approximation over the thickness of thin shells and neglecting transverse shear effects, developed a nonlinear model for incompressible hyperelastic material. Campello et al.[15] introduce the Rodrigues rotation vector to carry out the analysis of nonlinear hyperelastic shells using a neo-Hookean material model. Basar and Itskov[16] propose a numerical implementation of the Ogden material model via a variational procedure. The large strain and finite rotation fields are analyzed by introducing a six parametric shells kinematic. The absolute nodal coordinate formulation was adopted by Luo et al.[17] to carry out the static and dynamic nonlinear analysis of thin shells. The proposed approach is based on the Kirchhoff–Love hypotheses. Spherical and circular cylindrical shells were investigated by Song and Dai,[18] using a finite-strain shell theory. They employed a high-order expansion from the 3D equations for compressible hyperelastic materials. An extensible director kinematic is used by Betsch et al.[19] and Li et al.[20] for the analysis of compressible and incompressible hyperelastic shells, respectively. A nonlinear Lagrangian formulation was employed.

To the best of the authors' knowledge, much more attention was focused on thin shells made of hyperelastic materials, rather than their thick counterparts. The latter would require the adoption of more refined theories, which could eventually describe the through-the-thickness (both normal and shear) strains employing a refined approximation of the displacement field. More in general, when the thickness deformation plays a crucial role in the mechanical behavior of a structure, the adoption of higher-order theories is demanding. This is the case of thick shells and, in particular, of biological and rubber-soft materials, as outlined in many review articles ([21-24]). Moreover, for biological applications, multilayered structures are often adopted, and they represent typical cases when an accurate description of the transverse components is mandatory. An important contribution for the analysis of shells with higher-order models is given by Arbind and Reddy[25] which employed a general polynomial interpolation of the displacement field to develop of a general refined shell hyperelastic model. Moreover, Amabili et al.[26] developed a geometrically nonlinear model for incompressible cylindrical hyperelastic structures. By employing a 9-parameter theory, a higher-order description of the in-plane and out-of-plane strain components was carried out.

It can be said that the main difficulties when dealing with hyperelastic shells are due to the complexity of the formulation for a hyperelastic material and the derivation of the nonlinear governing equations for shells. In this context, the Carrera unified formulation (CUF)[27] represents a good framework. Due to its hierarchical nature, it is possible to build higher-order shell models by means of the so-called *fundamental nuclei* which, opportunely expanded, compose the stiffness matrix. The form of those does not depend on the theory order, which can be chosen by the user as input for the analysis. CUF has already been applied for the analysis of shell structures in the geometrical nonlinear field (see References [28 and 29]) and for hyperelastic structures (see Reference [30]). In this article, CUF is further extended to deal with hyperelastic thin and thick shell structures.

This work is organized as follows. An introduction to the geometric relation of shell structures is given in Section 2 in the curvilinear coordinate system. The hyperelastic constitutive law in the coupled form (following the Holzapfel[31] terminology) is described in Section 3. Section 4 describes the kinematics of the proposed nonlinear shell formulation and the derivation of the governing equations introducing the finite element method (FEM). The numerical results, proposed in Section 5, involve the analysis of cylindrical thick and thin shells made of compressible and incompressible hyperelastic materials. The article concludes by drawing the main conclusions. Also, appendix sections are provided, and they give the components of the linear and nonlinear differential operators and the material Jacobian tensor.

2 | GEOMETRICAL RELATIONS OF A SHELL IN AN ORTHOGONAL CURVILINEAR COORDINATE SYSTEM

2.1 | Reference configuration of a shell

Let us consider an arbitrarily curved shell as shown in Figure 1. The structure is considered to have a constant thickness h. The shell lays within a curvilinear coordinate system ξ^1, ξ^2, ξ^3, where ξ^3 lays along $\mathbf{n}$, which is the unit vector normal to
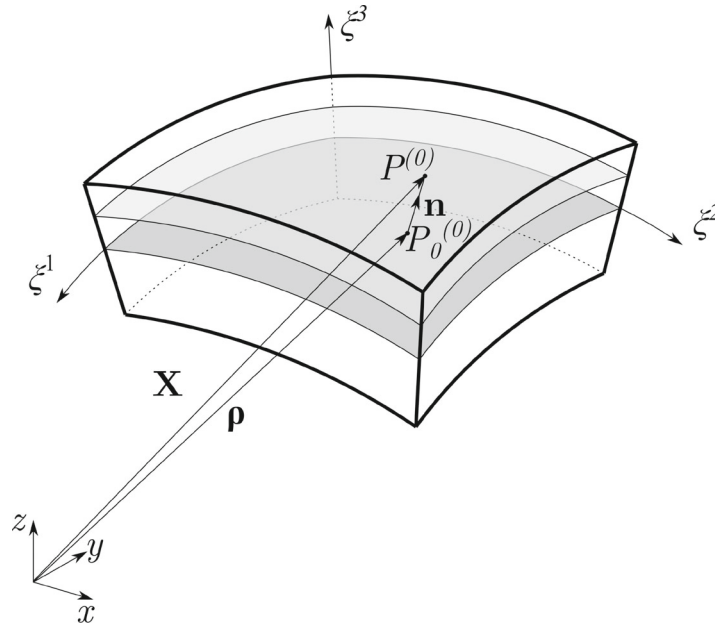
FIGURE 1   Geometry of an arbitrary shell in an orthogonal curvilinear coordinate system.

the surface that is defined by the two in-plane parametric curves ξ^1 and ξ^2. It is clear that $\xi^3 \in [-h/2; h/2]$. The relation between the position vectors $\mathbf{X}$ (point $P^{(0)}$) and $\boldsymbol{\rho}$ (point $P_0^{(0)}$) can be expressed as follows:

$$\mathbf{X}\left(\xi^1, \xi^2, \xi^3\right) = \boldsymbol{\rho}\left(\xi^1, \xi^2\right) + \xi^3 \mathbf{n}\left(\xi^1, \xi^2\right). \tag{1}$$

Starting from the position vector $\mathbf{X}$, the covariant base vectors $\mathbf{g}_i$ and it dual counterpart base vectors $\mathbf{g}^i$ can be derived as follows:

$$\mathbf{g}_i = \frac{\partial \mathbf{X}}{\partial \xi^i} = \mathbf{X}_{,i}, \quad \mathbf{g}_i \cdot \mathbf{g}^j = \delta_i^j,$$
$$g_{ij} = \mathbf{g}_i \cdot \mathbf{g}_j, \quad g^{ij} = \mathbf{g}^i \cdot \mathbf{g}^j, \tag{2}$$

where $(i = 1, 2, 3)$. Moreover, the partial derivative within a curvlinear coordinate system of a generic vector $\mathbf{A}$ reads as follows:

$$\frac{\partial \mathbf{A}}{\partial \xi^j} = A_{;j}^i \mathbf{g}_i = A_{i;j} \mathbf{g}^i, \tag{3}$$

where the spatial covariant derivative is conventionally expressed by the semicolon ";", and it is defined as follows:

$$A_{;j}^i = A_{,j}^i + A^m \Gamma_{jm}^i, \quad A_{i;j} = A_{i,j} - A_m \Gamma_{ji}^m. \tag{4}$$

Equation (4) introduces the Christoffel symbols, whose components can be expressed in the following:

$$\Gamma_{ij}^p = g^{kp} \Gamma_{ijk}, \quad \Gamma_{ijk} = g_{kl} \Gamma_{ij}^l = \frac{1}{2}\left(g_{ik,j} + g_{jk,i} - g_{ij,k}\right). \tag{5}$$

If the directions ξ^1 and ξ^2 are considered to lay along the curvatures of the shell structure, then the coordinate system results to be *orthogonal*, that is the considered case in the present study. Thus, $\mathbf{g}_i$ and $\mathbf{g}^i$ result to be orthogonal, and their modules are defined as follows:

$$\left|\mathbf{g}_i\right| = H_i = 1/\left|\mathbf{g}^i\right|, \quad (i = 1, 2, 3). \tag{6}$$

with H_i being the Lamé parameters of an arbitrary parallel surface of the shell. They are defined as follows:

$$
\begin{aligned}
H_1 &= A\left(1 + \xi^3/R_1\right), \\
H_2 &= B\left(1 + \xi^3/R_2\right), \\
H_3 &= 1,
\end{aligned}
\tag{7}
$$

where R_1 and R_2 are the principal curvature radii, whereas the mid-surface Lamé parameters are defined by A and B. In this research, cylindrical shells are examined, and, as a result, constant curvatures are presumed. Thus, both R_1 and R_2 are constant.

2.2 | Motion of a shell in the orthogonal curvilinear system

Consider the motion of a shell between two configurations, as depicted in Figure 2, where the position vector of the point in the final configuration is given by **x**. The displacement vector **u** can be expressed in the *total Lagrangian* description as follows:

$$
\mathbf{u} = \mathbf{x} - \mathbf{X} = u_i \mathbf{g}^i = u^i \mathbf{g}_i.
\tag{8}
$$

Therefore, the deformation gradient tensor **F** is defined as follows:

$$
\mathbf{F} = \nabla \mathbf{x} = \nabla(\mathbf{X} + \mathbf{u}) = \nabla \mathbf{X} + \nabla \mathbf{u} = \mathbf{I} + \nabla \mathbf{u} = \frac{\partial \mathbf{u}}{\partial \xi^j} \otimes \mathbf{g}^j,
\tag{9}
$$

where the $\otimes$ and ∇ symbols stand for the dyad operators and the gradient operator with respect to the reference configuration, respectively.

A set of orthogonal normalization vectors $\mathbf{e}_i$ is here introduced to simplify the analysis of physical problems, since $\mathbf{g}_i$ and $\mathbf{g}^i$ are not necessarily unit vectors in an orthogonal curvilinear coordinate system (see Equation (6)).

$$
\mathbf{e}_i = \mathbf{g}^i / \left| \mathbf{g}^i \right| = H_i \mathbf{g}^i.
\tag{10}
$$

Then, the displacement vector can be re-written, in terms of $\mathbf{e}_i$, as follows:

$$
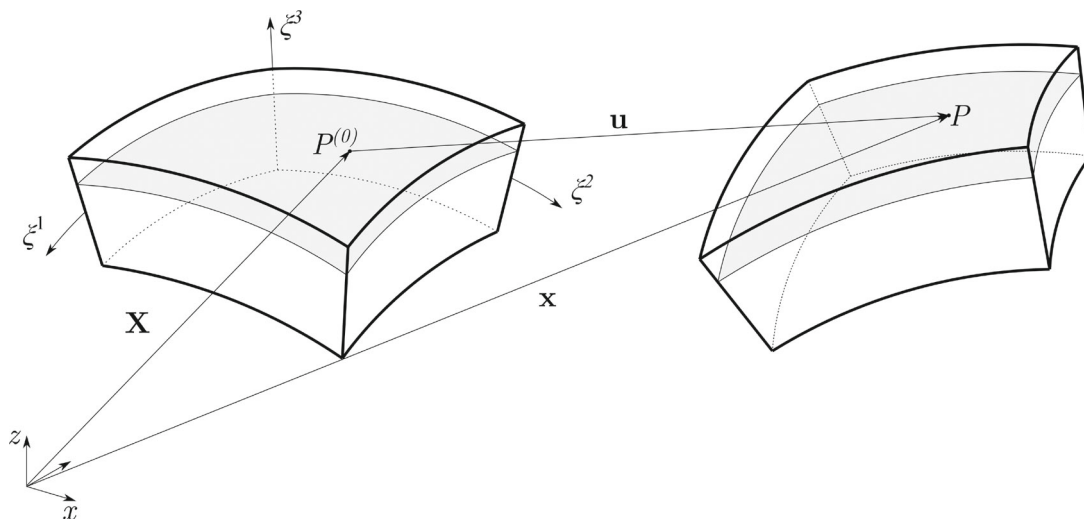\mathbf{u} = \tilde{u}_i \mathbf{e}_i,
\tag{11}
$$

FIGURE 2 Motion of an arbitrary shell in an orthogonal curvilinear coordinate system.

where $\tilde{u}_i$ express the *physical* components. Introducing Equations (8) and (10) into (11), one has

$$u_i = H_i \tilde{u}_i. \tag{12}$$

Thus, considering Equation (3), Equation (9) can be expressed as follows:

$$\mathbf{F}_{ij} = \mathbf{I}_{ij} + \left[\left(\frac{\partial H_j}{\partial \xi^i} \tilde{u}_j + H_j \frac{\partial \tilde{u}_j}{\partial \xi^i} \right) \frac{\mathbf{e}_i}{H_i} \otimes \frac{\mathbf{e}_j}{H_j} \right] - \sum_{m=1}^{3} \left[\left(H_m \tilde{u}_m \Gamma_{ij}^m \right) \frac{\mathbf{e}_i}{H_i} \otimes \frac{\mathbf{e}_j}{H_j} \right]. \tag{13}$$

In this work, we consider ξ^1 and ξ^2 as the *arc-length coordinates*, and in this work they are referred to as α and β, respectively (z for ξ^3), and consequently, $A = B = 1$.

The 3×3 deformation gradient tensor $\mathbf{F}$ of Equation (9) is given by

$$\mathbf{F} = \begin{bmatrix} \frac{u_{\alpha,\alpha}}{H_\alpha} + \frac{u_z}{H_\alpha R_\alpha} + 1 & \frac{u_{\alpha,\beta}}{H_\beta} & u_{\alpha,z} \\[2mm] \frac{u_{\beta,\alpha}}{H_\alpha} & \frac{u_{\beta,\beta}}{H_\beta} + \frac{u_z}{H_\beta R_\beta} + 1 & u_{\beta,z} \\[2mm] \frac{u_{z,\alpha}}{H_\alpha} - \frac{u_\alpha}{H_\alpha R_\alpha} & \frac{u_{z,\beta}}{H_\beta} - \frac{u_\beta}{H_\beta R_\beta} & u_{z,z} + 1 \end{bmatrix}. \tag{14}$$

The Green–Lagrange strain tensor $\mathbf{E}$ can be expressed as follows:

$$\mathbf{E} = \left(\mathbf{F}^{\mathrm{T}} \mathbf{F} - \mathbf{I} \right)/2 = \frac{1}{2} \left[\nabla \mathbf{u} + (\nabla \mathbf{u})^{\mathrm{T}} + (\nabla \mathbf{u})^{\mathrm{T}} \cdot \nabla \mathbf{u} \right] = \mathbf{E}_l + \mathbf{E}_{nl}, \tag{15}$$

where the transpose is indicated by the superscript "T." The linear $\mathbf{E}_l$ and nonlinear $\mathbf{E}_{nl}$ components of the strain $\mathbf{E}$ in Equation (9) can be written as follows:

$$\mathbf{E}_l = \frac{1}{2} \left[\nabla \mathbf{u} + (\nabla \mathbf{u})^{\mathrm{T}} \right] = \frac{1}{2} \left(u_{i;j} + u_{j;i} \right) \mathbf{g}^i \otimes \mathbf{g}^j = \frac{1}{2} \left(u_{j,i} + u_{i,j} - 2u_m \Gamma_{ij}^m \right) \mathbf{g}^i \otimes \mathbf{g}^j, \tag{16}$$

and

$$\begin{aligned} \mathbf{E}_{nl} &= \frac{1}{2} (\nabla \mathbf{u})^{\mathrm{T}} \cdot \nabla \mathbf{u} = \frac{1}{2} u_{k;i} u_{;j}^k \mathbf{g}^i \otimes \mathbf{g}^j \\ &= \frac{1}{2} \left(u_{k,i} u_{;j}^k - u_m \Gamma_{ki}^m u_{;j}^k + u_{k,i} u^n \Gamma_{nj}^k - u_m \Gamma_{ki}^m u^n \Gamma_{nj}^k \right) \mathbf{g}^i \otimes \mathbf{g}^j, \end{aligned} \tag{17}$$

Subsequently, Equations (16) and (17) can be rearranged in a matrix form as follows:

$$\mathbf{E} = \mathbf{E}_l + \mathbf{E}_{nl} = (\mathbf{b}_l + \mathbf{b}_{nl})\mathbf{u}, \tag{18}$$

where $\mathbf{u}$ and $\mathbf{E}$ can be defined as

$$\mathbf{u}(\alpha, \beta, z) = \left\{ u_\alpha \quad u_\beta \quad u_z \right\}^{\mathrm{T}}, \quad \mathbf{E} = \left\{ E_{\alpha\alpha} \quad E_{\beta\beta} \quad E_{zz} \quad E_{\alpha z} \quad E_{\beta z} \quad E_{\alpha\beta} \right\}^{\mathrm{T}}, \tag{19}$$

The 6×3 linear and nonlinear differential operators $\mathbf{b}_l$ and $\mathbf{b}_{nl}$ in Equation (18) are given in Appendix A.

3 | HYPERELASTIC CONSTITUTIVE LAW

In the present work, isotropic hyperelastic behavior is described adopting a neo-Hookean strain-energy function Ψ. In general, the strain energy function Ψ can be written in terms of the invariants (I_1, I_2, I_3) of the $\mathbf{C} = \mathbf{F}^{\mathrm{T}} \mathbf{F}$ right Cauchy–Green tensor as follows:

$$\Psi = \Psi(I_1(\mathbf{C}), I_2(\mathbf{C}), I_3(\mathbf{C})), \tag{20}$$

where the invariants are defined as follows:

$$I_1 = \mathrm{tr}(\mathbf{C}),$$

$$I_2 = \frac{1}{2}((\mathrm{tr}(\mathbf{C}))^2 - \mathrm{tr}(\mathbf{C}^2)), \tag{21}$$

$$I_3 = \det(\mathbf{C}),$$

where $\mathrm{tr}(\cdot)$ and $\det(\cdot)$ represent the trace and the determinant operators.

The constitutive law is expressed as a differential relation between Ψ and the second Piola-Kirchhoff (PK2) stress tensor as follows:

$$\mathbf{S} = 2\frac{\partial\Psi(\mathbf{C})}{\partial\mathbf{C}} = \frac{\partial\Psi(\mathbf{C})}{\partial I_1}\frac{\partial I_1}{\partial\mathbf{C}} + \frac{\partial\Psi(\mathbf{C})}{\partial I_2}\frac{\partial I_2}{\partial\mathbf{C}} + \frac{\partial\Psi(\mathbf{C})}{\partial I_3}\frac{\partial I_3}{\partial\mathbf{C}}, \tag{22}$$

where

$$\frac{\partial I_1}{\partial\mathbf{C}} = \frac{\partial\mathrm{tr}\,\mathbf{C}}{\partial\mathbf{C}} = \frac{\partial(\mathbf{I}:\mathbf{C})}{\partial\mathbf{C}} = \mathbf{I},$$

$$\frac{\partial I_2}{\partial\mathbf{C}} = \frac{1}{2}\left(2\mathrm{tr}\,\mathbf{C}\,\mathbf{I} - \frac{\partial\mathrm{tr}\mathbf{C}^2}{\partial\mathbf{C}}\right) = I_1\mathbf{I} - \mathbf{C}, \tag{23}$$

$$\frac{\partial I_3}{\partial\mathbf{C}} = I_3\mathbf{C}^{-1}.$$

Introducing Equation (23) into Equation (22), one has the final expression of the PK2 tensor,

$$\mathbf{S} = 2\frac{\partial\Psi(\mathbf{C})}{\partial\mathbf{C}} = 2\left[\left(\frac{\partial\Psi}{\partial I_1} + I_1\frac{\partial\Psi}{\partial I_2}\right)\mathbf{I} - \frac{\partial\Psi}{\partial I_2}\mathbf{C} + I_3\frac{\partial\Psi}{\partial I_3}\mathbf{C}^{-1}\right]. \tag{24}$$

The material Jacobian tensor is given in Appendix B.

4 | TWO-DIMENSIONAL (2D) UNIFIED SHELL FINITE ELEMENTS

4.1 | Unified shell finite element

In this work, the 2D shell finite element is built recalling the CUF. According to CUF, the 3D displacement field of Equation (19) can be derived as a set of in-plane functions over the α and β directions and thickness functions over the thickness domain z. α, β and z are the physical coordinates. Specifically, $\mathbf{u}$ can be written as follows:

$$\mathbf{u}(\alpha, \beta, z) = F_\tau(z)\mathbf{u}_\tau(\alpha, \beta), \tag{25}$$

where $\tau = 0, 1, \ldots, N$, with N being the order of expansion functions F_τ. The repeated subscript τ indicates the summation. In this article, cubic and quadratic expansion functions, based on three-point and four-point Lagrange polynomials, are employed. Following the notation introduced by Carrera,[32] they are recalled as Lagrange Displacement LDo, which stands for Lagrange expansion with Displacement unknowns of order o (2 and 3 for quadratic and cubic expansion, respectively). For the sake of completeness, the case of a LD2, namely a quadratic expansion, is reported hereafter

$$u_\alpha = F_1 u_{\alpha 1} + F_2 u_{\alpha 2} + F_3 u_{\alpha 3},$$

$$u_\beta = F_1 u_{\beta 1} + F_2 u_{\beta 2} + F_3 u_{\beta 3}, \tag{26}$$

$$u_z = F_1 u_{z1} + F_2 u_{z2} + F_3 u_{z3},$$

where

$$
\begin{aligned}
F_1 &= \frac{1}{2}(s^2 + ss_1), \\
F_2 &= -s^2 + 1, \\
F_3 &= \frac{1}{2}(s^2 + ss_3),
\end{aligned}
\tag{27}
$$

where s vary from 1 to -1, whereas s_1 and s_3 correspond to the position of the Lagrange points in the natural coordinate. The relation between the natural and physical coordinates can be found in many books, see Reference 27. On the other hand, for the α-β domain discretization, FEM is recalled. After discretizing the shell mid-plane in planar finite elements, the generalized displacement vector $\mathbf{u}_\tau(\alpha, \beta)$ can be expressed in the following:

$$
\mathbf{u}_\tau(\alpha, \beta) = N_i(\alpha, \beta)\mathbf{q}_{\tau i},
\tag{28}
$$

where $i = 1, 2, \ldots, p + 1$, with p representing the order of the shape functions N_i. The vector of the FE nodal parameters $\mathbf{q}_{sj}$ is written as

$$
\mathbf{q}_{\tau i} = \left\{ q_{\alpha_{\tau i}} \quad q_{\beta_{\tau i}} \quad q_{z_{\tau i}} \right\}^{\mathrm{T}}.
\tag{29}
$$

Note that the finite element interpolation is expressed by using global coordinates in Equation (28). However, stiffness terms as detailed in Section 4.2 are derived by integrating both the shape functions N_i and the theory approximation expansions F_τ in the natural domain, as in classical FEM. In this work, nine-node bi-quadratic FEs (Q9) are adopted as shape functions.

Figure 3 depicts the discretization of an arbitrary shell structure, where the expansion function F_τ and the shape function N_i are highlighted in red and blue, respectively.

Note that, introducing CUF Equation (27) and FEM (28) into Equation (18), the resultant strain vector can be expressed as follows:

$$
\mathbf{E} = (\mathbf{B}_l^{\tau i} + \mathbf{B}_{nl}^{\tau i})\mathbf{q}_{\tau i},
\tag{30}
$$

where $\mathbf{B}_l^{\tau i}$ and $\mathbf{B}_{nl}^{\tau i}$ are the linear and nonlinear algebraic matrices. Interested readers can find more details about $\mathbf{B}_l^{\tau i}$ and $\mathbf{B}_{nl}^{\tau i}$ in Reference 28.

4.2 | Nonlinear governing equations

In the present work, the derivation of the nonlinear governing equation is conducted recalling the PVDs. It can be written as follows:

$$
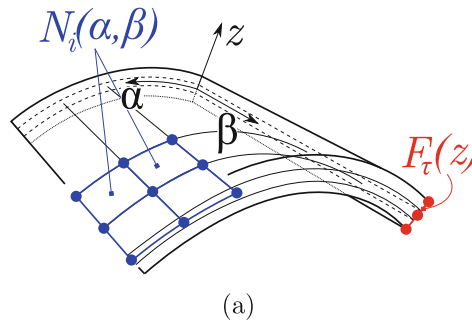\delta L_{\mathrm{int}} = \delta L_{\mathrm{ext}},
\tag{31}
$$

(a)

FIGURE 3 2D shell model. Shape function N_j in blue and expansion function F_s in red.

where δL_{int} and δL_{ext} are the virtual variation of the internal strain energy and the external loads, respectively, with δ denoting the variation. The virtual variation of the internal work can be expressed as follows:

$$\delta L_{\text{int}} = \int_V \delta \mathbf{E}^T \mathbf{S} \, dV, \tag{32}$$

where V is the volume of the body, and

$$\delta \mathbf{E} = \delta((\mathbf{B}_l^{\tau i} + \mathbf{B}_{nl}^{\tau i})\mathbf{q}_{\tau i}) = (\mathbf{B}_l^{\tau i} + 2\mathbf{B}_{nl}^{\tau i})\delta \mathbf{q}_{\tau i}. \tag{33}$$

Introducing Equation (33) into Equation (32), one has

$$\delta L_{int} = \int_\Omega \delta \mathbf{q}_{\tau i}^T (\mathbf{B}_l^{\tau i} + 2\mathbf{B}_{nl}^{\tau i})^T \mathbf{S} \, \mathrm{dV} = \delta \mathbf{q}_{\tau i}^T [\int_V (\mathbf{B}_l^{\tau i} + 2\mathbf{B}_{nl}^{\tau i})^T \mathbf{S} \mathrm{dV}] = \delta \mathbf{q}_{\tau i}^T \mathbf{F}_{int}^{\tau i}, \tag{34}$$

where $\mathbf{F}_{int}^{\tau i}$ is the 3×1 fundamental nucleus of the internal forces vector:

$$\mathbf{F}_{int}^{\tau i} = \int_\Omega (\mathbf{B}_l^{\tau i} + 2\mathbf{B}_{nl}^{\tau i})^T \mathbf{S} dV. \tag{35}$$

The expression of the external load vector is computed from the definition of the virtual variation of the work made by external forces. Omitting some mathematical derivations, we have

$$\delta L_{ext} = \delta \mathbf{q}_{\tau i}^T \mathbf{F}_{ext}^{\tau i}. \tag{36}$$

Finally, introducing Equations (34) and (36) into (31), the nonlinear equation holds

$$\mathbf{F}_{int}^{\tau i} = \mathbf{F}_{ext}^{\tau i}. \tag{37}$$

Equation (37) represents a geometrically nonlinear systems, and it is typically computed adopting a linearization technique. In this article, the employed scheme is the Newton–Raphson method, according to which, the nonlinear governing equations are expressed as follows:

$$\boldsymbol{\varphi}_{res} \equiv \mathbf{F}_{int}^{\tau i} - \mathbf{F}_{ext}^{\tau i} = 0, \tag{38}$$

where the *residual nodal forces* vector is expressed in $\boldsymbol{\varphi}_{res}$. One can use a known $(\mathbf{q}, \mathbf{p})$ solution to linearize Equation (38) by expanding $\boldsymbol{\varphi}_{res}$ in Taylor's series. Therefore,

$$\boldsymbol{\varphi}_{res}(\mathbf{q} + \delta\mathbf{q}, \mathbf{p} + \delta\mathbf{p}) = \boldsymbol{\varphi}_{res}(\mathbf{q}, \mathbf{p}) + \frac{\partial \boldsymbol{\varphi}_{res}}{\partial \mathbf{q}} \delta\mathbf{q} + \frac{\partial \boldsymbol{\varphi}_{res}}{\partial \mathbf{p}} \delta\lambda \, \mathbf{p}_{ref} = 0, \tag{39}$$

where $\frac{\partial \boldsymbol{\varphi}_{res}}{\partial \mathbf{q}} = \mathbf{K}_T$ represents the *tangent* stiffness matrix. The external load is assumed to change directly with the vector of the reference loadings $\mathbf{p}_{ref}$ with a variation rate expressed by λ, defined as the load-scaling parameter, i.e. $\mathbf{p} = \lambda \, \mathbf{p}_{ref}$. Since λ is a variable, an additional constraint equation is required and this is given by a relation constraining both $\delta\mathbf{q}$ and $\delta\lambda$). Finally, one has

$$\begin{cases} \mathbf{K}_T \, \delta\mathbf{q} = \delta\lambda \, \mathbf{p}_{ref} - \boldsymbol{\varphi}_{res}, \\ c(\delta\mathbf{q}, \delta\lambda) = 0. \end{cases} \tag{40}$$

In this work, a path-following technique is adopted as the constraint equation. In particular, an arc-length method is utilized in this work, see Criesfield[33,34] and Carrera.[35] It is important to underline that $\mathbf{K}_T$ is derived from the linearization of the equilibrium equations.[36] This corresponds to the linearization of the virtual variation of the work made by internal forces in the case of conservative cases, as follows

$$\delta(\delta L_{\text{int}}) = \int_V \delta \mathbf{E}^T \mathbf{S} \, \mathrm{dV} = \delta \mathbf{q}_{\tau i}^T \mathbf{K}_T^{ij\tau s} \delta \mathbf{q}_{sj}, \tag{41}$$

where $\mathbf{K}_T^{ij\tau s}$ represents the 3×3 *fundamental nucleus*, that is, the basic building block for the formulation of the total tangent stiffness matrix.

5 | NUMERICAL RESULTS

The numerical results concern three examples taken from the literature. Each of them is analyzed considering a neo-Hookean strain energy function. In particular, the study cases involve a curved arch and both thick and thin cylinders subjected to line and point load. For the thin cylinder subjected to a point load, both compressible and incompressible material configurations are considered, and the obtained results are compared to those from literature, when available.

5.1 | Curved arch

As a first example, the behavior of a compressible soft curved arch is investigated. Figure 4 shows the geometrical characteristics and boundary condition of the structure, with r_i and r_e equal to 9 and 10 mm, respectively, and a = 1 mm. Then, the structure can be considered as thick ($r_e/a = 10$), and can be modeled using the proposed shell finite element thanks to its higher-order capability. The structure is clamped and subjected to an external pressure oriented by 45° with respect to the normal of the surface. The study case is taken from Hassani et al.,[37] and the neo-Hookean material model is described in the following strain energy function:

$$\Psi(\mathbf{C}) = \frac{\mu}{2}(I_1 - 3) - \frac{\mu}{2}\log I_3 + \frac{k}{2}(\sqrt{I_3} - 1)^2 \tag{42}$$

where μ and k are the shear and bulk modulus, respectively. Their values are $\mu = 80.194$ N/mm^2 and $k = 120.291$ N/mm^2, so that the material is compressible.

A preliminary convergence analysis is carried out, in order to establish a reliable mathematical model. Figure 5 shows the results. Clearly, the 120 Q9 and 2 LD3 approximation can be considered a converged mathematical model. Its total number of Degrees of Freedom (DOFs) is 11907. The nonlinear static equilibrium curve is reported in Figure 6, along with some of the deformed configurations. A good match between the proposed model solution and the reference results is guaranteed.

5.2 | Cylindrical shell subjected to line loading

The hyperelastic cylindrical structure shown in Figure 7 is considered as the second analysis case. The geometric properties are $r = 9$ cm and $L = 15$ cm. Both thick and thin configurations are considered, with thicknesses t and t_2 equal
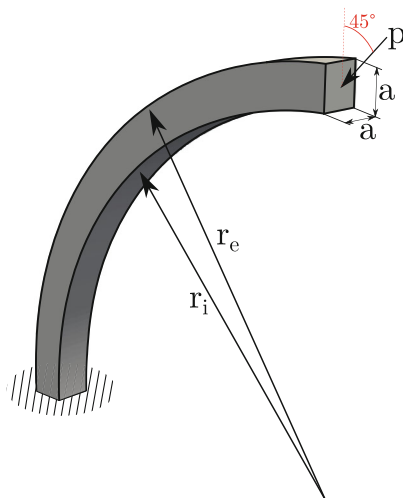

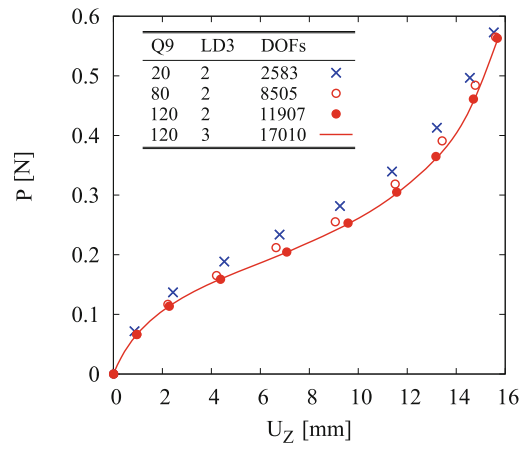**FIGURE 4** Geometric properties of the curved arch. Study case taken from Hassani et al.[37]

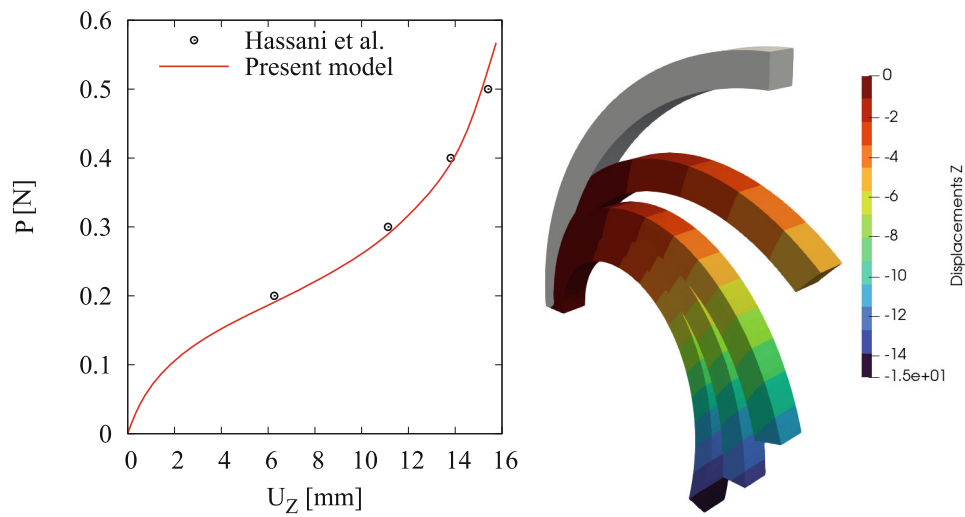**FIGURE 5** Convergence analysis of the arch subjected to an external pressure.

FIGURE 6 Nonlinear static equilibrium curve of the arch subjected to an external pressure. Some deformed configurations are reported. Reference results from Hassani et al.[37]
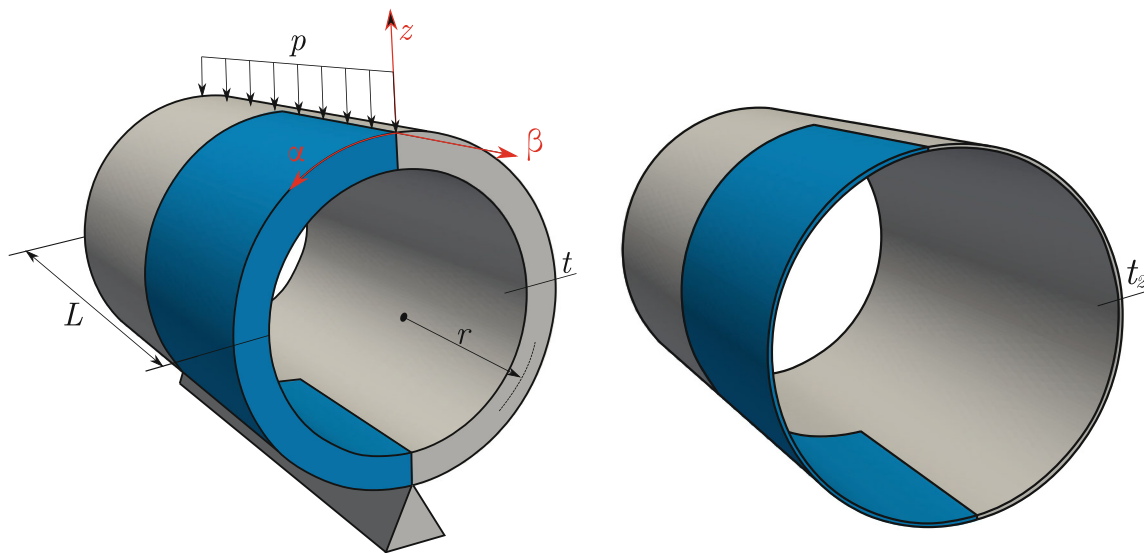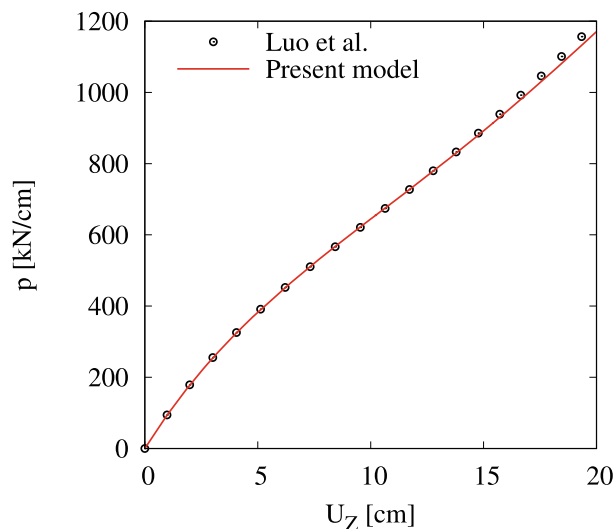

FIGURE 7 Study case of the cylinder under line load.

FIGURE 8 Nonlinear analysis of the cylinder under line load. Thickness equals to 2 cm. Reference result from Luo et al.[17]
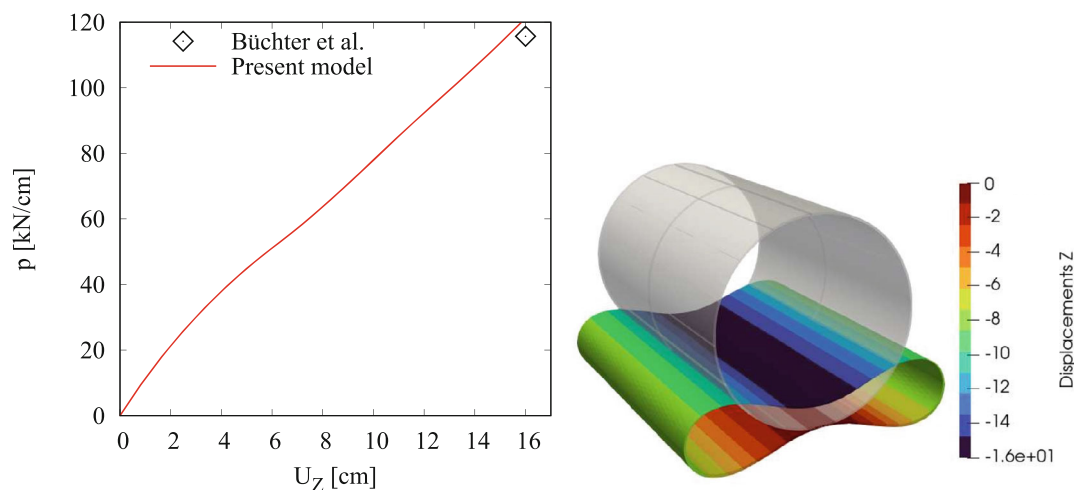

FIGURE 9 Nonlinear analysis of the cylinder under line load. Thickness equals to 0.2 cm. Reference result from Büchter et al.[38]

to 2 and 0.2 cm, respectively. A neo-Hookean material model is adopted with the same strain energy function Φ adopted in Reference[17] with shear modulus $\mu = 6000\,\text{kN/cm}^2$ and bulk modulus $k = 280{,}000\,\text{kN/cm}^2$. For symmetry reasons, only one quarter of the structure is considered (depicted in blue in 7). A 4×10 Q9 mesh is adopted, along with one LD2 on the thickness direction, resulting in a total of 1701 DOFs. The thick cylinder was analyzed as the first case, and the results are compared to reference ones from Luo et al.[17]

The nonlinear equilibrium curve is shown in Figure 8, proving a perfect match with the reference solution. Moreover, the thin cylinder is considered. The available reference solution is from Büchter et al.,[38] where a single equilibrium state in the force *vs* displacement graph is provided (see Figure 9). The solution obtained with the present model is reported in the same graph, and a consistent match with literature results is demonstrated. In the same figure, the deformed configuration at maximum vertical displacement equals 16 cm is provided.

5.3 | Cylindrical shell subjected to pinching loading

As the final case, a cylindrical shell with rigid end diaphragms is subjected to pinching point load P, as shown in Figure 10. This example was studied in References 39 and 40 by using different approaches, whereas the results chosen
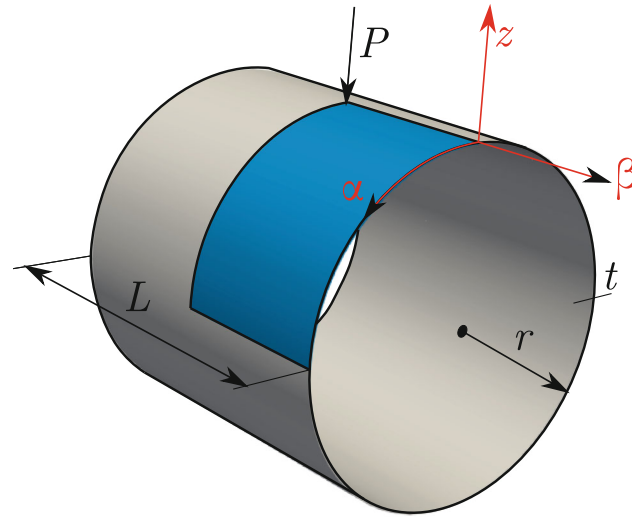
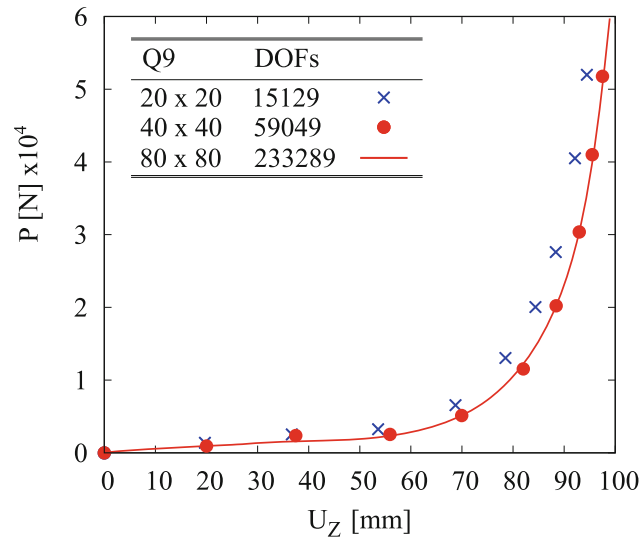**FIGURE 10** Study case of the cylinder under pinching point load.

FIGURE 11 Convergence analysis of the cylinder under pinching point load. For each model one LD2 is adopted over the thickness direction.

here as reference are from Luo et al.[17] The radius, length, and thickness of the cylindrical shell are $r = 100$ mm, $L = 200$ mm, and $t = 1$ mm, respectively. The boundary condition of rigid diaphragms is enforced on the two edges of the cylindrical shell. This means that the displacements of the edges of the cylindrical shell are constrained except along the longitudinal direction. Thanks to the symmetrical property of the problem, only one octant of the shell is studied.

A convergence analysis is carried out as a preliminary investigation to assess the mathematical model, and the results are shown in Figure 11. Clearly, the 40×40 Q9 mathematical model can be considered as converged, and is used for the subsequent investigations. The number of DOFs is 59049. Both compressible and nearly incompressible neo-Hookean material models are considered here, with Poisson's ratios $v = 0.3$ and $v = 0.499$, respectively.

The obtained results in terms of nonlinear equilibrium curve are shown in Figure 12 and, in the compressible case, they match well with the reference solution from Luo et al.[17] Moreover, Figure 13 depicts some of the deformed shapes of the cylindrical shell at the nonlinear static load steps of maximum vertical displacement equals to 57, 76, 86, and 96 mm, respectively.
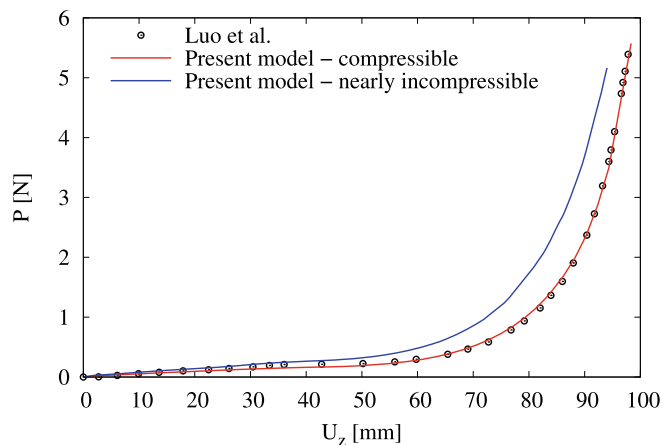
FIGURE 12 Nonlinear analysis of the cylinder under pinching point load. Reference solution from Luo et al.[17] for compressible case.
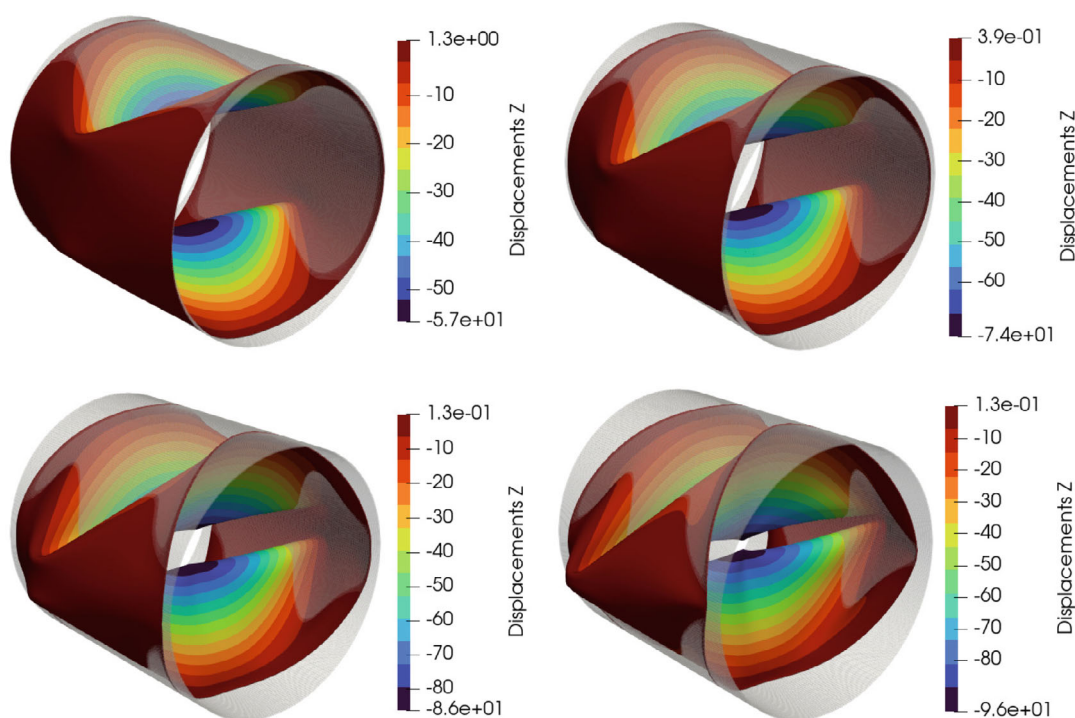

FIGURE 13 Deformed shapes of the cylinder under pinching point load.

6 | CONCLUSIONS

This article proposed a unified 2D shell finite element for the analysis of hyperelastic structures. The model is based on the CUF, which, combined with the finite element method (FEM), allows to generate higher-order shell models. The deformation gradient and the Green–Lagrange strain tensors are derived in an orthogonal curvilinear coordinate system, whereas the Jacobian material matrix is expressed in its coupled formulation of hyperelastic constitutive law. The principle of virtual displacement (PVD) is recalled to generate the nonlinear governing equations which are finally solved using an algorithm based on the Newton–Raphson linearization and the arc-length methods. The proposed model was used to analyze a curved arch and cylinders (both thick and thin) with a Neo-Hookean strain energy function. The results obtained from this study are compared to existing literature, proving that the proposed higher-order model is a viable choice for simulating solid shells. These are traditionally modeled using three-dimensional (3D) solid elements, resulting in a high number of degrees of freedom and geometric inconsistencies. Furthermore, as no locking or stability issues were encountered in the simulations, the use of these higher-order models holds the potential to mitigate such problems.

Future work will deal with the extension of the present model to deal with fully incompressible materials, eventually exploring mixed or hybrid formulation to contrast volumetric locking, anisotropic soft materials and multi-physics.

DATA AVAILABILITY STATEMENT

The data that support the findings of this study are available from the authors upon reasonable request.

ORCID

A. Pagani [ORCID] https://orcid.org/0000-0001-9074-2558
E. Carrera [ORCID] https://orcid.org/0000-0002-6911-7763

REFERENCES

1. Lü X, Jiang J, Wang H, et al. Sensitivity-compensated micro-pressure flexible sensor for aerospace vehicle. *Sensors*. 2018;19(1):72.
2. Sadeghnejad S, Elyasi N, Farahmand F, Vossughi G, Sadr Hosseini SM. Hyperelastic modeling of sino-nasal tissue for haptic neurosurgery simulation. *Sci Iran*. 2020;27(3):1266-1276.
3. Holzapfel GA. Determination of material models for arterial walls from uniaxial extension tests and histological structure. *J Theoret Biol*. 2006;238(2):290-302.
4. Treloar LRG. *The Physics of Rubber Elasticity*. Oxford University Press; 1975.
5. Shabana AA. *Computational Continuum Mechanics*. John Wiley & Sons; 2018.
6. Basar Y, Ding Y. Finite-element analysis of hyperelastic thin shells with large strains. *Computational Mechanics*. 1996;18(3):200-214.
7. Tamadapu G, DasGupta A. Finite inflation of a hyperelastic toroidal membrane over a cylindrical rim. *International Journal of Solids and Structures*. 2014;51(2):430-439.
8. Kiendl J, Hsu M-C, Wu MCH, Reali A. Isogeometric kirchhoff–love shell formulations for general hyperelastic materials. *Computer Methods in Applied Mechanics and Engineering*. 2015;291:280-303.
9. Xu F, Johnson EL, Wang C, et al. Computational investigation of left ventricular hemodynamics following bioprosthetic aortic and mitral valve replacement. *Mechanics Research Communications*. 2021;112:103604.
10. Holzapfel GA, Eberlein R, Wriggers P, Weizsäcker HW. Large strain analysis of soft biological membranes: Formulation and finite element analysis. *Computer Methods in Applied Mechanics and Engineering*. 1996;132(1-2):45-61.
11. Cerda E, Ravi-Chandar K, Mahadevan L. Wrinkling of an elastic sheet under tension. *Nature*. 2002;419(6907):579-580.
12. Fu C, Wang T, Xu F, Huo Y, Potier-Ferry M. A modeling and resolution framework for wrinkling in hyperelastic sheets at finite membrane strain. *Journal of the Mechanics and Physics of Solids*. 2019;124:446-470.
13. Cerda E, Mahadevan L. Geometry and physics of wrinkling. *Physical Review Letters*. 2003;90(7):74302.
14. Love AEH. The small free vibrations and deformation of a thin elastic shell. *Proceedings of the Royal Society of London Series*. 1887;I(43):352-353.
15. Campello EMB, Pimenta PM, Wriggers P. An exact conserving algorithm for nonlinear dynamics with rotational dofs and general hyperelasticity. part 2: shells. *Computational Mechanics*. 2011;48:195-211.
16. Başar Y, Itskov M. Finite element formulation of the ogden material model with application to rubber-like shells. *International Journal for Numerical Methods in Engineering*. 1998;42(7):1279-1305.
17. Luo K, Liu C, Tian Q, Hu H. Nonlinear static and dynamic analysis of hyper-elastic thin shells via the absolute nodal coordinate formulation. *Nonlinear Dynamics*. 2016;85(2):949-971.
18. Song Z, Dai H-H. On a consistent finite-strain shell theory based on 3-d nonlinear elasticity. *International Journal of Solids and Structures*. 2016;97:137-149.
19. Betsch P, Gruttmann F, Stein E. A 4-node finite shell element for the implementation of general hyperelastic 3d-elasticity at finite strains. *Computer Methods in Applied Mechanics and Engineering*. 1996;130(1-2):57-79.
20. Li Y, Dai H-H, Wang J. On a consistent finite-strain shell theory for incompressible hyperelastic materials. *Mathematics and Mechanics of Solids*. 2019;24(5):1320-1339.
21. Beatty MF. Topics in finite elasticity: hyperelasticity of rubber, elastomers, and biological tissues—with examples. *Applied Mechanics Reviews*. 1987;40(12):1699-1734.
22. Attard MM. Finite strain–isotropic hyperelasticity. *International Journal of Solids and Structures*. 2003;40(17):4353-4378.
23. Fu YB, Ogden RW. *Nonlinear Elasticity: Theory and Applications*. Cambridge University Press; 2001.
24. Horgan CO, Polignone DA. Cavitation in nonlinearly elastic solids: a review. *Appl Mech Rev*. 1995;48(8):471-485.
25. Arbind A, Reddy JN. A general higher-order shell theory for compressible isotropic hyperelastic materials using orthonormal moving frame. *Int J Numer Methods Eng*. 2021;122(1):235-269.
26. Amabili M, Breslavsky ID, Reddy JN. Nonlinear higher-order shell theory for incompressible biological hyperelastic materials. *Comput Methods Appl Mech Eng*. 2019;346:841-861.
27. Carrera E, Cinefra M, Petrolo M, Zappino E. *Finite Element Analysis of Structures Through Unified Formulation*. John Wiley & Sons; 2014.
28. Wu B, Pagani A, Chen WQ, Carrera E. Geometrically nonlinear refined shell theories by carrera unified formulation. *Mech Adv Mater Struct*. 2021;28(16):1721-1741.
29. Carrera E, Pagani A, Augello R, Wu B. Popular benchmarks of nonlinear shell analysis solved by 1d and 2d cuf-based finite elements. *Mech Adv Mater Struct*. 2020;27(13):1098-1109.

30. Pagani A, Carrera E. Unified one-dimensional finite element for the analysis of hyperelastic soft materials and structures. *Mech Adv Mater Struct*. 2023;30(2):342-355.

31. Holzapfel GA. *Nonlinear Solid Mechanics: A Continuum Approach for Engineering Science*. John Wiley & Sons; 2000.

32. Carrera E. Theories and finite elements for multilayered plates and shells: a unified compact formulation with numerical assessment and benchmarking. *Arch Comput Methods Eng*. 2003;10:215-296.

33. Crisfield MA. A fast incremental/iterative solution procedure that handles "snap-through". *Computational Methods in Nonlinear Structural and Solid Mechanics*. Elsevier; 1981:55-62.

34. Crisfield MA. An arc-length method including line searches and accelerations. *Int J Numer Methods Eng*. 1983;19(9):1269-1289.

35. Carrera E. A study on arc-length-type methods and their operation failures illustrated by a simple model. *Comput Struct*. 1994;50(2):217-229.

36. Zienkiewicz OC, Taylor RL. *The Finite Element Method for Solid and Structural Mechanics*. Butterworth-Heinemann; 2005.

37. Hassani R, Ansari R, Rouhi H. Large deformation analysis of 2d hyperelastic bodies based on the compressible nonlinear elasticity: A numerical variational method. *Int J Non-Linear Mech*. 2019;116:39-54.

38. Büchter N, Ramm E, Roehl D. Three-dimensional extension of non-linear shell formulation based on the enhanced assumed strain concept. *Int J Numer Methods Eng*. 1994;37(15):2551-2568.

39. Ivannikov V, Tiago C, Pimenta PM. Meshless implementation of the geometrically exact Kirchhoff–Love shell theory. *Int J Numer Methods Eng*. 2014;100(1):1-39.

40. Diaby A, Wielgosz C. Buckling and wrinkling of prestressed membranes. *Finite Elements Anal Design*. 2006;42(11):992-1001.

APPENDIX A. LINEAR AND NONLINEAR DIFFERENTIAL OPERATORS

The 6×3 linear and nonlinear differential operators $\mathbf{b}_l$ and $\mathbf{b}_{nl}$ in Equation (18) are reported here.

$$
\mathbf{b}_l = \begin{bmatrix}
\frac{\partial_\alpha}{H_\alpha} & 0 & \frac{1}{H_\alpha R_\alpha} \\
0 & \frac{\partial_\beta}{H_\beta} & \frac{1}{H_\beta R_\beta} \\
0 & 0 & \partial_z \\
\partial_z - \frac{1}{H_\alpha R_\alpha} & 0 & \frac{\partial_\alpha}{H_\alpha} \\
0 & \partial_z - \frac{1}{H_\beta R_\beta} & \frac{\partial_\beta}{H_\beta} \\
\frac{\partial_\beta}{H_\beta} & \frac{\partial_\alpha}{H_\alpha} & 0
\end{bmatrix},
\tag{A1}
$$

and

$$
\mathbf{b}_{nl} = \begin{bmatrix}
\frac{1}{2H_\alpha^2}\left[(\partial_\alpha)^2 + \frac{2\,u_z\partial_\alpha}{R_\alpha} + \frac{u_\alpha}{R_\alpha^2}\right] & \frac{(\partial_\alpha)^2}{2H_\alpha^2} & \frac{1}{2H_\alpha^2}\left[(\partial_\alpha)^2 - \frac{2\,u_\alpha\partial_\alpha}{R_\alpha} + \frac{u_z}{R_\alpha^2}\right] \\
\frac{(\partial_\beta)^2}{2H_\beta^2} & \frac{1}{2H_\beta^2}\left[(\partial_\beta)^2 + \frac{2\,u_z\partial_\beta}{R_\beta} + \frac{u_\beta}{R_\beta^2}\right] & \frac{1}{2H_\beta^2}\left[(\partial_\beta)^2 - \frac{2\,u_\beta\partial_\beta}{R_\beta} + \frac{u_z}{R_\beta^2}\right] \\
\frac{1}{2}(\partial_z)^2 & \frac{1}{2}(\partial_z)^2 & \frac{1}{2}(\partial_z)^2 \\
\frac{1}{H_\alpha}\left(\partial_\alpha\partial_z + \frac{u_z\partial_z}{R_\alpha}\right) & \frac{\partial_\alpha\partial_z}{H_\alpha} & \frac{1}{H_\alpha}\left(\partial_\alpha\partial_z - \frac{u_\alpha\partial_z}{R_\alpha}\right) \\
\frac{\partial_\beta\partial_z}{H_\beta} & \frac{1}{H_\beta}\left(\partial_\beta\partial_z + \frac{u_z\partial_z}{R_\beta}\right) & \frac{1}{H_\beta}\left(\partial_\beta\partial_z - \frac{u_\beta\partial_z}{R_\beta}\right) \\
\frac{1}{H_\alpha H_\beta}\left(\partial_\alpha\partial_\beta + \frac{u_z\partial_\beta}{R_\alpha} + \frac{u_\beta}{R_\alpha R_\beta}\right) & \frac{1}{H_\alpha H_\beta}\left(\partial_\alpha\partial_\beta + \frac{u_z\partial_\alpha}{R_\beta}\right) & \frac{1}{H_\alpha H_\beta}\left(\partial_\alpha\partial_\beta - \frac{u_\alpha\partial_\beta}{R_\alpha} - \frac{u_\beta\partial_\alpha}{R_\beta}\right)
\end{bmatrix},
\tag{A2}
$$

in which $\partial_\alpha = \partial(\cdot)/\partial\alpha$, $\partial_\beta = \partial(\cdot)/\partial\beta$, and $\partial_z = \partial(\cdot)/\partial z$.

APPENDIX B. MATERIAL JACOBIAN TENSOR

The material Jacobian tensor, in its most generic form, which is recalled as coupled formulation in Reference 31, is expressed in terms of principal invariants as follows:

$$
\begin{aligned}
\mathcal{C} = 2\frac{\partial \mathbf{S}(\mathbf{C})}{\partial \mathbf{C}} &= \frac{\partial \mathbf{S}(\mathbf{E})}{\partial \mathbf{E}} = 4\frac{\partial^2 \Psi}{\partial \mathbf{C}\partial \mathbf{C}} \\
&= 4\left(\frac{\partial^2 \Psi}{\partial I_1^2} + 2I_1\frac{\partial^2 \Psi}{\partial I_1 \partial I_2} + \frac{\partial \Psi}{\partial I_2} + I_1^2\frac{\partial^2 \Psi}{\partial I_2^2} \right)\mathbf{I} \otimes \mathbf{I} \\
&\quad - 4\left(\frac{\partial^2 \Psi}{\partial I_1 \partial I_2} + I_1\frac{\partial^2 \Psi}{\partial I_2^2} \right)(\mathbf{I} \otimes \mathbf{C} + \mathbf{C} \otimes \mathbf{I}) \\
&\quad + 4\left(I_3\frac{\partial^2 \Psi}{\partial I_1 \partial I_3} + I_1 I_3\frac{\partial^2 \Psi}{\partial I_2 \partial I_3} \right)(\mathbf{I} \otimes \mathbf{C}^{-1} + \mathbf{C}^{-1} \otimes \mathbf{I}) \\
&\quad + 4\frac{\partial^2 \Psi}{\partial I_2^2}\mathbf{C} \otimes \mathbf{C} \\
&\quad - 4I_3\frac{\partial^2 \Psi}{\partial I_2 \partial I_3}(\mathbf{C} \otimes \mathbf{C}^{-1} + \mathbf{C}^{-1} \otimes \mathbf{C}) \\
&\quad + 4\left(I_3\frac{\partial \Psi}{\partial I_3} + I_3^2\frac{\partial^2 \Psi}{\partial I_3^2} \right)\mathbf{C}^{-1} \otimes \mathbf{C}^{-1} \\
&\quad - 4I_3\frac{\partial \Psi}{\partial I_3}\mathbf{C}^{-1} \odot \mathbf{C}^{-1} \\
&\quad - 4\frac{\partial \Psi}{\partial I_2}\mathcal{S}
\end{aligned}
\tag{B1}
$$

where $\mathcal{S}$ is function of the fourth-order unit tensor.